

# Optimization of dispersion in hollow-core photonic crystal fibers filled with toluene

Duc Hoang Trong <sup>1</sup>, Thong Hoang Minh <sup>2</sup>, Thuy Nguyen Thi <sup>1\*</sup>

<sup>1</sup> University of Education, Hue University, 34 Le Loi Street, Hue City, Viet Nam

<sup>2</sup> Hoa Binh Xuan Loc College, Bien Hoa City, Dong Nai Province, Viet Nam

\* Correspondence to Thuy Nguyen Thi <ntthuy@hueuni.edu.vn>

(Received: 9 August 2022; Accepted: 03 November 2022)

**Abstract.** In this work, we investigate in detail the dispersion of SiO<sub>2</sub>-based photonic crystal fibers with C<sub>7</sub>H<sub>8</sub>-infiltrated hollow cores. By cleverly modifying the air hole diameters and lattice constants in the structural design, we achieved ultra-flat near-zero dispersion as small as 0.462 ps/(nm.km) and diverse dispersion properties of PCFs, which are very beneficial for supercontinuum generation. Based on the analysis of the simulation results, we propose three optimal structures with small and flat dispersion capable of generating a broad and smooth SC spectrum. The results of our study will be very useful for fabricating fibers in low-cost all-fiber laser systems.

**Keywords:** PCF, C<sub>7</sub>H<sub>8</sub>, Ultra-flat dispersion, diverse dispersion, Supercontinuum generation

## 1 Introduction

Supercontinuum (SC) generation is a process where a narrow laser pulse is propagated through a strong nonlinear device and converted into light with a very broad spectral bandwidth. Since it was first reported by Alfano [1] until now, the research on generating SC using photonic crystal fibers (PCFs) has attracted many research groups around the world due to its wide application range, such as nonlinear microscope [2], spectroscopy [3, 4], pulse compression [5], high-resolution optical coherence tomography [6], frequency metrology [7], gas sensing [8], optical communication systems [9], biology [10], etc. PCF is a new type of optical fiber and has the capability to confine light in its core region, which is not possible with conventional optical fibers. The flexibility in structural design and dispersion control makes PCF an attractive nonlinear medium for researchers in SC generation. The combination of the selection of geometries for the

PCF structure, including adjustment of the lattice parameters [12–16], and the permeation of the hollow core of the PCF with highly nonlinear liquids such as chloroform, nitrobenzene, carbon disulfide, carbon tetrachloride, and tetrachloroethylene [17–21] are common ways to design the PCF.

PCFs with ultra-flattened, near-zero dispersion have been the target of many researchers to generate SC with large bandwidth and high coherence. By appropriately reducing the diameter of the core-neighboring air hole ring, Abdelkader Medjouri *et al.* [22] obtained an ultra-flattened chromatic dispersion as small as  $\pm 0.66$  ps/nm/km over a broadband of 400 nm with high nonlinearity and ultra-low confinement loss. This PCF generates the flat SC spectrum with an FWHM of 600 nm and 25 cm of fiber length. The work [23] introduced a PCF with a subwavelength air hole in the core region and an air hole arrangement in the cladding region and achieved

an ultra-flattened normal dispersion within  $-72.4$  to  $-73.15$  ps/(nm.km) from 1750 to 2350 nm wavelength. A SC bandwidth of 238 nm can be obtained by using 50 cm of fiber. By using other substrates to replace silica, Huang [24] proposed a modified hexagonal tellurite PCF with broadband ultra-flattened dispersion; the dispersion can be kept within 60.47 ps/(nm.km) to 61.33 ps/(nm.km) from 2.15 to 2.85  $\mu\text{m}$  wavelength. The SC spectrum covering 2000–4900 nm and the dispersive wave located near 933 nm can be produced by using 5 cm fiber. The results in Ref. [25] show that the PCF structure with lead silicate ethanol displays extremely low dispersion with a value that is less than 5 ps/(nm.km) and an SC bandwidth of 2784 nm, which can be obtained for the peak power of 5 kW. The results of the above studies show that the SC generation efficiency depends strongly on the ultra-flattened near-zero dispersion of these PCFs.

In this study, a circular silica-based PCF with a toluene-filled core, the diameter of the air holes, and the lattice constant of the first ring are designed differently from other rings in order to improve optical properties such as dispersion, nonlinear coefficient, effective mode area, and attenuation. Toluene ( $\text{C}_7\text{H}_8$ ) has been chosen to infiltrate the PCF because it has a high nonlinear refractive index and low toxicity. Its nonlinear refractive index is  $n_2 = 16.8 \times 10^{-19} \text{ m}^2 \cdot \text{W}^{-1}$  [26], which is 60 times higher compared to silica ( $n_2 = 2.79 \times 10^{-20} \text{ m}^2 \cdot \text{W}^{-1}$ ) [27]. Several SC studies based on toluene-infiltrated PCF have demonstrated the ability to control dispersion by reducing the diameters of the first-ring air holes near the core [28, 29], but ultra-flattened near-zero dispersion has not been achieved. We chose the circular lattices to design the PCF structure because of their high symmetry, and therefore light is strongly restricted to the core. Moreover, most of the previous publications on PCF using hexagonal and circular lattices have not been studied much.

With such a design, we achieve an ultra-flattened near-zero dispersion as small as 0.462 ps/(nm.km) for the wavelength range of 500 nm. Moreover, the dispersion characteristic of the PCF can be easily controlled by adjusting the filling factor  $d_1/\Lambda$ .

## 2 Numerical modeling of the toluene-core PCFs

All the  $\text{C}_7\text{H}_8$ -filled PCF structures are modeled by using Lumerical Mode Solutions (LMS) with the full-vector finite-difference eigenmode (FDE) method to achieve the field intensity profile of the fundamental mode of the PCFs. The process of FDE utilizes the Maxwell wave equation and the boundary condition for simulation is a perfectly matched layer, which allows strong absorption of the outgoing waves from the computational region without any reflection. The typical way of controlling the physical parameters is by changing the geometry of the PCF structures, such as the lattice constant and the air hole diameter. The schematic part of the designed fiber has been shown in Fig.1a. The cladding consists of 8 layers of air holes, which are periodically arranged in a regular circular structure with toluene infiltration in the core. The diameter of the innermost air holes of the cladding is  $d_1$ , while the diameter of the air holes in layers 2–8 is  $d_2$ . The linear filling factor of the cladding is defined as  $d_1/\Lambda$  for the first ring and  $d_2/\Lambda$  for the other rings ( $\Lambda$  is the lattice constant). The work [21, 22, 29, 30] shows that the dispersion properties, including flatness and zero-dispersion wavelength shift, are dominated by the size of the air holes in the first ring of the cladding, but the size of other rings is responsible for the low attenuation of the fundamental mode and even the higher modes. To our knowledge, no work has mentioned the influence of the lattice constant of the first ring on the control of the dispersion characteristics of

PCF. Therefore, for this simulation, the distance from the center of the core to the air-holes of the first inner ring is chosen as  $\Lambda_1 = 1.099\Lambda$  while the distance between the other rings is kept as  $\Lambda$ . We keep the same value of 0.95 for the filling factor  $d_2/\Lambda$  (but  $d_1/\Lambda$  varies from 0.3 to 0.65) and use the following lattice constants  $\Lambda$ : 0.9  $\mu\text{m}$ , 1.0  $\mu\text{m}$ . By skillfully tuning such lattice parameters, PCF has demonstrated good confinement of light in the core (Fig. 1b).

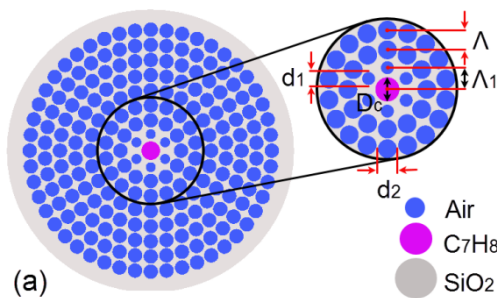


Fig. 1. a. The geometrical structures of PCF with toluene-core

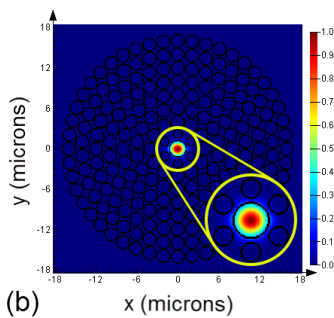


Fig. 1. b. The light is well confined in the core of PCF

The real parts of the refractive index of toluene and fused silica used in this paper versus wavelength are shown in Fig. 1c. Cauchy's equation [31] shows the dependence of refractive index characteristics on wavelength for toluene:

$$n_{\text{Toluene}}^2(\lambda) = 2.161659124 + 0.000495188\lambda^2 + 0.021381790\lambda^{-2} + 0.000058838\lambda^{-4} + 0.000087632\lambda^{-6} \quad (1)$$

Fused silica is selected as the background material in all the designs of these PCFs, and the refractive index can be obtained using the Sellmeier formula [32]:

$$n_{\text{Fused silica}}^2(\lambda) = 1 + \frac{0.6694226\lambda^2}{\lambda^2 - 4.4801 \times 10^{-3}} + \frac{0.4345839\lambda^2}{\lambda^2 - 1.3285 \times 10^{-2}} + \frac{0.8716947\lambda^2}{\lambda^2 - 95.341482} \quad (2),$$

where  $\lambda$  is the excitation wavelength in micrometers,  $n(\lambda)$  is the wavelength-dependent linear refractive index of materials.

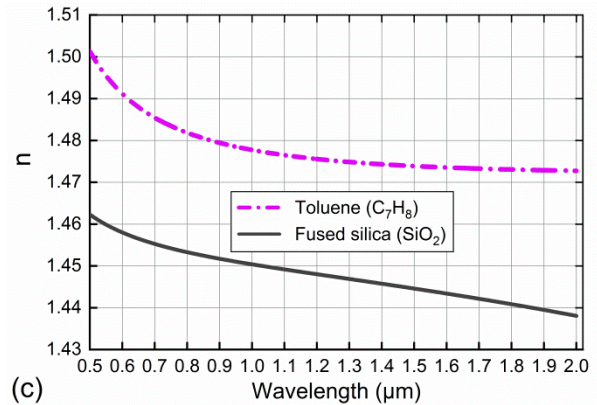


Fig. 1. c. Real parts of the refractive index of toluene and fused silica

### 3 Optimization of dispersion in the toluene-core PCFs

The dispersion parameters corresponding to the designed fibers are calculated by using the formula [33],

$$D = -\frac{\lambda}{c} \frac{d^2 \text{Re}[n_{\text{eff}}]}{d\lambda^2} \quad (3),$$

where  $\text{Re}[n_{\text{eff}}]$  is the real part of  $n_{\text{eff}}$ , which is the effective index of a guided mode calculated by the FDE method, and  $c$  is the velocity of light in a vacuum.

The large difference in refractive index between the core and the mantle is essential for the light modes to be well confined in the core, which is important for the optimization of the dispersion of the PCF. The relationship between the effective refractive index and the investigated wavelength is displayed in Fig. 2.

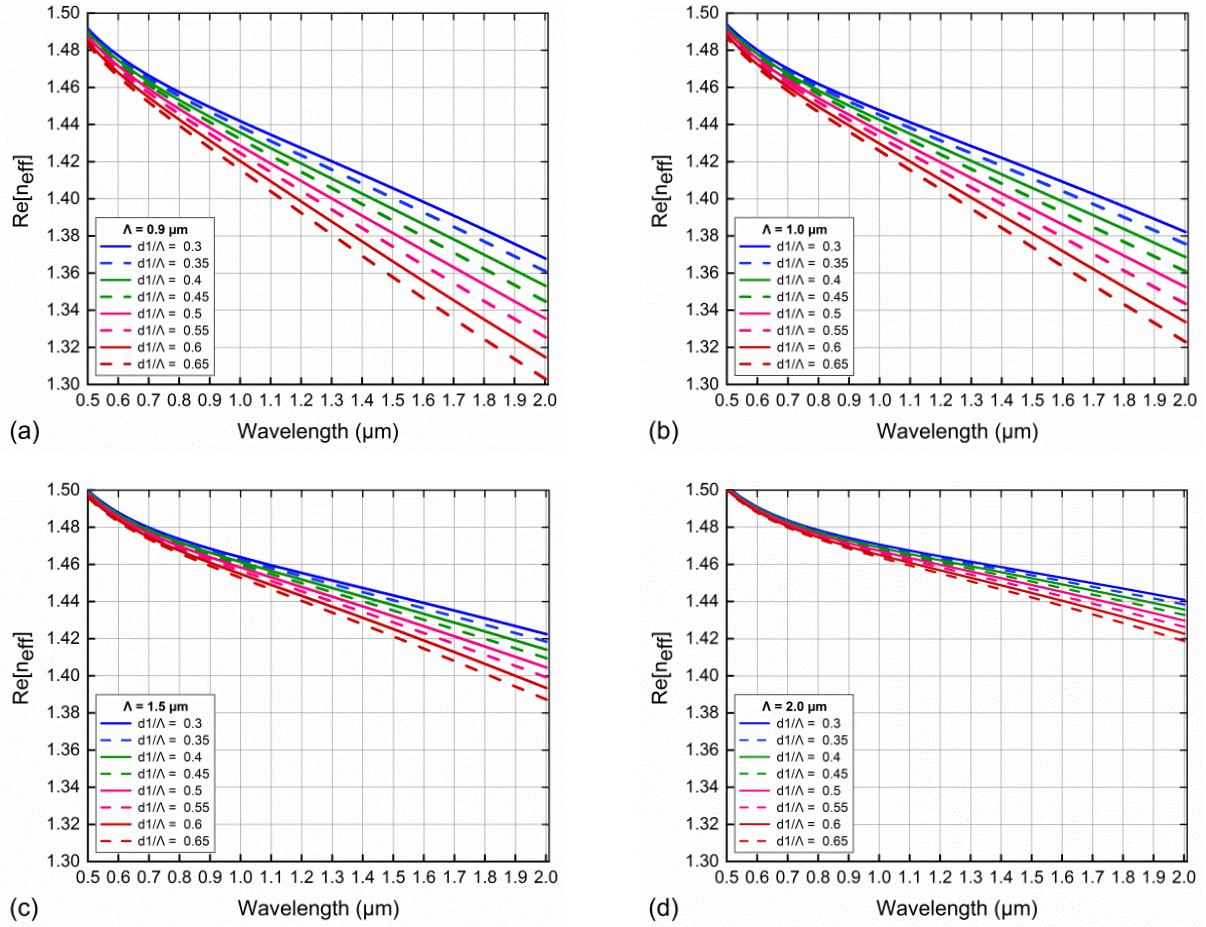


**Fig. 2.** The real part of effective refractive index as a function of wavelength with various  $d_1/\Lambda$  and  $\Lambda = 0.9 \mu\text{m}$  (a),  $\Lambda = 1.0 \mu\text{m}$  (b),  $\Lambda = 1.5 \mu\text{m}$  (c), and  $\Lambda = 2.0 \mu\text{m}$  (d)

In all cases, as wavelength increases, the real part of the effective refractive index ( $\text{Re}[n_{\text{eff}}]$ ) decreases monotonically. In the low-frequency region,  $\text{Re}[n_{\text{eff}}]$  has a small value due to the leakage of light modes either into the cladding or between the air holes. When  $d_1/\Lambda$  is fixed, the real part of the effective refractive index increases with the lattice constant  $\Lambda$ . Meanwhile, the change of  $d_1/\Lambda$  will strongly affect the value of  $\text{Re}[n_{\text{eff}}]$  if the lattice constant  $\Lambda$  is fixed. In particular, the decrease of  $d_1/\Lambda$  causes  $\text{Re}[n_{\text{eff}}]$  to rise. The ability

to confine light in very small-diameter cores is worse than that in large-diameter cores. Because the core diameter depends on both  $d_1$  and the lattice constant  $\Lambda$  and is determined by the formula:  $D_{\text{core}} = 2\Lambda - 1.2d_1$ . However, if the core of PCF is too large, mode leakage will increase. Therefore, the limit of increase in core diameter must be kept in mind during the design of the PCF in order to minimize light leakage into the cladding.

**Table 1.** The value of the  $\text{Re}[n_{\text{eff}}]$  of the effective refraction index with various  $d_1/\Lambda$  and  $\Lambda$  at 1.55  $\mu\text{m}$  wavelength.

| $d_1/\Lambda$ | $\text{Re}[n_{\text{eff}}]$ |                             |                             |                             |
|---------------|-----------------------------|-----------------------------|-----------------------------|-----------------------------|
|               | $\Lambda = 0.9 \mu\text{m}$ | $\Lambda = 1.0 \mu\text{m}$ | $\Lambda = 1.5 \mu\text{m}$ | $\Lambda = 2.0 \mu\text{m}$ |
| 0.3           | 1.402                       | 1.412                       | 1.441                       | 1.454                       |
| 0.35          | 1.397                       | 1.408                       | 1.439                       | 1.453                       |
| 0.4           | 1.391                       | 1.402                       | 1.436                       | 1.451                       |
| 0.45          | 1.384                       | 1.397                       | 1.433                       | 1.449                       |
| 0.5           | 1.377                       | 1.390                       | 1.429                       | 1.447                       |
| 0.55          | 1.369                       | 1.384                       | 1.426                       | 1.445                       |
| 0.6           | 1.361                       | 1.377                       | 1.422                       | 1.443                       |
| 0.65          | 1.352                       | 1.369                       | 1.418                       | 1.440                       |

Tab. 1 indicates the value of the real part of the effective refraction index of PCFs with various  $d_1/\Lambda$  values at 1.55  $\mu\text{m}$  wavelength, which is the common pumping wavelength of the laser in SC generation. The maximum and minimum values of  $\text{Re}[n_{\text{eff}}]$  are 1.454 and 1.352 with  $\Lambda = 2.0 \mu\text{m}$ ;  $d_1/\Lambda = 0.3$  and  $\Lambda = 0.9 \mu\text{m}$ ;  $d_1/\Lambda = 0.65$ , respectively. The small difference between the two refractive index values for both cases is 0.102, proving that the light modes are well confined in the core of the toluene-infiltrated PCFs. This promises that we will obtain the expected dispersion properties.

The dispersion characteristic of PCF causes a change in the optical pulse per unit distance of the propagation length, so a PCF with suitable dispersion properties for SC generation is always the aim of researchers. The dependence of dispersion on wavelength for different values of  $d_1/\Lambda$  and  $\Lambda$  as shown in Fig.3. Both anomalous and all-normal dispersion regimes are found with a larger shift of ZDWs towards the longer wavelength region. For the smaller lattice

constant ( $\Lambda = 0.9 \mu\text{m}$ , Fig.3a), PCFs exhibit anomalous dispersion with one ZDW when  $d_1/\Lambda$  is less than 0.5. For the other case of  $d_1/\Lambda$ , the dispersion is completely located in the all-normal dispersion profile, and the decreasing values of the filling factor  $d_1/\Lambda$  (0.65 to 0.5) make the all-normal dispersions more and more flat and close to the zero-dispersion. Among them, the dispersion curve is the flattest when  $d_1/\Lambda = 0.5$ ; this curve will shift very close to the zero-dispersion as  $\Lambda$  increases (Fig.3b), which is very beneficial for the generation of SC with a broader and flatter spectrum [22–25]. For  $\Lambda = 1.0 \mu\text{m}$ , Fig.3b also presents the diversity in the dispersion characteristics of the PCFs. In this case, all-normal and anomalous dispersions with one and two ZDWs are observed. Very interestingly, an anomalous ultra-flattened near-zero dispersion, as small as 0.462 ps/(nm.km) over a broadband of 500 nm, is achieved in the investigated wavelength region when  $d_1/\Lambda = 0.5$ . This is an outstanding advantage that some previous publications on liquid-infiltrated PCFs have not yet achieved [17, 20, 22, 28–29]. The slope of the dispersion changes drastically for a variation of

the filling factor, i.e., the change in air-hole diameter, as also shown in Fig. 3a and 3b. The interaction between waveguide dispersion and material dispersion is responsible for this effect. For smaller  $d_1/\Lambda$ , material dispersion plays a major role, while the waveguide effect dominates for higher  $d_1/\Lambda$ . Besides, varying  $d_1/\Lambda$  and  $\Lambda$  also influences the shift of ZDW of PCF, this is manifested in Tab. 2. Shifting the ZDW toward

longer wavelengths in PCFs has an important role for soliton-driven supercontinuum by low-cost and short-pulse lasers with the pump wavelength chosen to be larger but closer to the ZDW. In the case  $\Lambda = 0.9 \mu\text{m}$  and  $d_1/\Lambda = 0.45$ , the value of ZDW is  $1.494 \mu\text{m}$ , which is approximate to the common pump wavelength ( $1.55 \mu\text{m}$ ) in SC-based generation based silica-PCF.

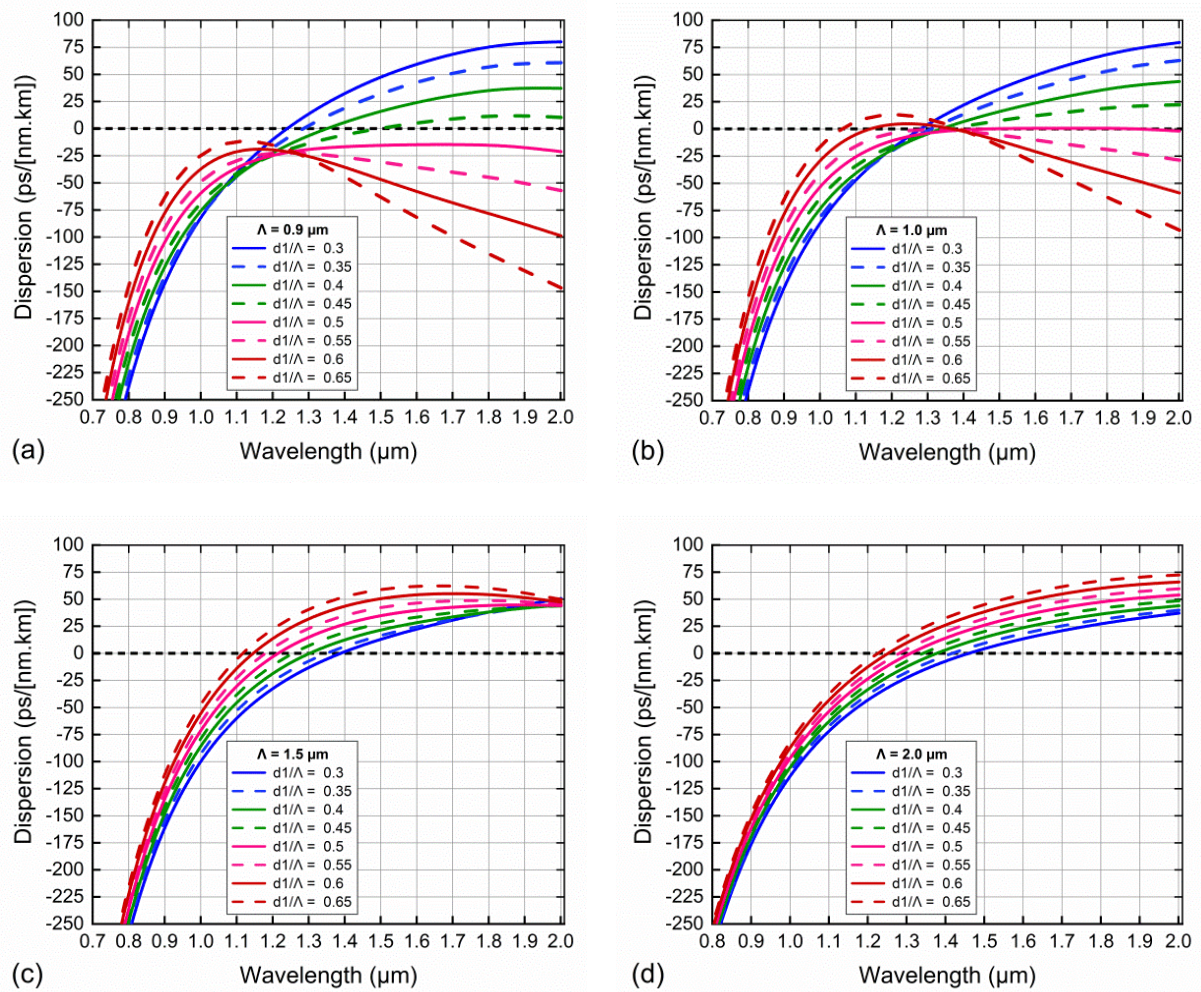


Fig. 3. The dispersion characteristics of toluene-core PCFs with various  $d_1/\Lambda$  and  $\Lambda = 0.9 \mu\text{m}$  (a),  $\Lambda = 1.0 \mu\text{m}$  (b),  $\Lambda = 1.5 \mu\text{m}$  (c), and  $\Lambda = 2.0 \mu\text{m}$  (d)

**Table 2.** The values of ZDW of toluene-core PCFs with various values of  $d_1/\Lambda$  and  $\Lambda$

| $d_1/\Lambda$ | $\Lambda = 0.9$ ( $\mu\text{m}$ ) | $\Lambda = 1.0$ ( $\mu\text{m}$ ) |       | $\Lambda = 1.5$ ( $\mu\text{m}$ ) | $\Lambda = 2.0$ ( $\mu\text{m}$ ) |
|---------------|-----------------------------------|-----------------------------------|-------|-----------------------------------|-----------------------------------|
|               | ZDWs1                             | ZDWs1                             | ZDWs2 | ZDWs1                             | ZDWs1                             |
| 0.3           | 1.239                             | 1.280                             |       | 1.388                             | 1.458                             |
| 0.35          | 1.284                             | 1.308                             |       | 1.349                             | 1.417                             |
| 0.4           | 1.350                             | 1.337                             |       | 1.300                             | 1.375                             |
| 0.45          | 1.494                             | 1.363                             |       | 1.256                             | 1.342                             |
| 0.5           |                                   | 1.455                             | 1.893 | 1.215                             | 1.309                             |
| 0.55          |                                   |                                   |       | 1.178                             | 1.280                             |
| 0.6           |                                   | 1.137                             | 1.373 | 1.145                             | 1.252                             |
| 0.65          |                                   | 1.061                             | 1.390 | 1.116                             | 1.225                             |

When  $\Lambda$  is larger ( $\Lambda = 1.5 \mu\text{m}$  and  $2.0 \mu\text{m}$ ), all dispersion curves intersect the horizontal axis, indicating that PCFs only exist in anomalous dispersion regimes with one ZDW. Furthermore, the dispersion value at a given wavelength increases with the increase of  $d_1/\Lambda$ . This results in ZDWs shifting towards shorter wavelengths. Therefore, if we keep an eye on the optimal structure corresponding to the anomalous dispersion, in this case, we should choose PCFs with a small  $d_1/\Lambda$ .

In our simulation, the difference in distances from the core center to the air holes of the first and other rings in the cladding is the main factor governing the flatness of the dispersion characteristic. To demonstrate this, we compare the dispersion characteristics of the toluene-core PCFs with the following lattice parameters:

\* The dispersion characteristic of PCFs with  $\Lambda = 1.0 \mu\text{m}$ , refers to [29], is shown in Fig. 4, where the distances from the core center to the air holes of the first and other rings are the same as  $\Lambda$ .

\* Fig.3b displays the dispersion characteristic of PCFs with  $\Lambda = 1.0 \mu\text{m}$ , where the

distance from the core center to the air holes of the first ring is  $\Lambda_1 = 1.099\Lambda$  and the distance between the air holes of the other rings is  $\Lambda$ .

Fig. 4 and Fig.3b verify that the dispersion characteristics of the PCFs in this work are flatter. Very interestingly, we achieve an ultra-flattened near-zero dispersion with  $\Lambda = 1.0 \mu\text{m}$  and  $d_1/\Lambda = 0.5$ .

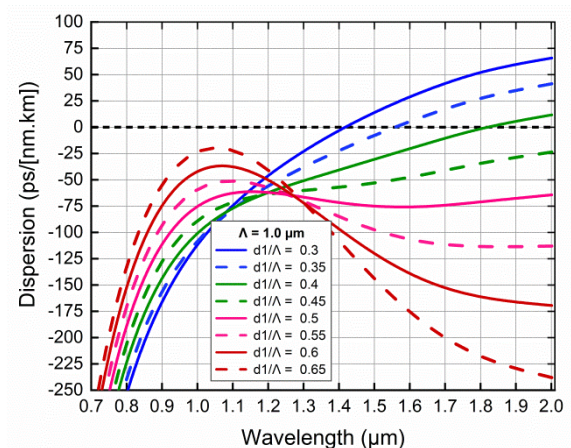


**Fig. 4.** The dispersion characteristics of toluene-core PCFs with various values of  $d_1/\Lambda$ ,  $\Lambda_1 = \Lambda$  and  $\Lambda = 1.0 \mu\text{m}$  [29]

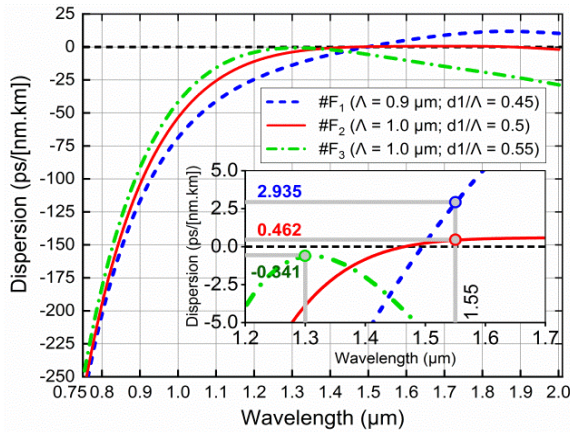


**Fig. 5.** The dispersion characteristics of proposed PCFs

The propagation of a narrow input pulse excited at a specified wavelength in a nonlinear medium such as PCF with different dispersion characteristics determines the characteristics of the SC spectrum. First, a smooth and broad spectrum is achieved in PCFs with an all-normal flat dispersion regime. However, in this case, the spectral expansion is limited due to phase self-modulation effects. So, peak power is a factor that needs to be considered carefully. Second, the low anomalous dispersion near ZDW provides the generation of a broader SC spectrum due to its soliton effects despite the low peak power, but the spectrum is often noisy [34]. Based on the above simulation results, we propose three optimal PCFs suitable for the generation of SC, namely #F<sub>1</sub>, #F<sub>2</sub>, and #F<sub>3</sub>. These structures, which exhibit good flatness dispersion and are close to the zero-dispersion curve in the investigated wavelength

region, are manifested in Fig. 5.

The first fiber #F<sub>1</sub> ( $\Lambda = 0.9 \mu\text{m}$  and  $d_1/\Lambda = 0.45$ ), has anomalous dispersion, which is expected to produce the highly coherent SC pulses in the regime of anomalous dispersion with a pump wavelength of  $1.55 \mu\text{m}$ . This fiber was selected because it has a ZDW of  $1.494 \mu\text{m}$ , which is the closest to the wavelength used for pumping. Another reason is that the calculated dispersion at  $1.55 \mu\text{m}$  equals  $2.935 \text{ ps}/(\text{nm.km})$ , which is also the smallest value for all dispersion characteristics computed for structures with  $\Lambda = 0.9 \mu\text{m}$  at  $1.55 \mu\text{m}$ . #F<sub>1</sub> fiber can offer broad soliton-induced SC generation.

The outstanding advantage of second fiber #F<sub>2</sub> is that it has an ultra-flattened near-zero dispersion and an anomalous dispersion regime with two ZDWs. Furthermore, the pump wavelength is  $1.55 \mu\text{m}$ , near the first ZDW of the dispersion curve, and the value of the dispersion is  $0.462 \text{ ps}/(\text{nm.km})$ , which is small enough for high SC efficiency. Therefore, the structure with  $\Lambda = 1.0 \mu\text{m}$  and  $d_1/\Lambda = 0.5$  was selected as the most optimal fiber, which was used for SC to achieve the broadest spectrum with low peak power.

#F<sub>3</sub> fiber with  $\Lambda = 1.0 \mu\text{m}$  and  $d_1/\Lambda = 0.55$  has an all-normal dispersion regime. The value of anomalous dispersion is  $-0.341 \text{ ps}/(\text{nm.km})$  at the pump wavelength of  $1.3 \mu\text{m}$ , near the local maximum point of the dispersion curve. This fiber can provide a broad and smooth SC spectrum.

**Table 3.** The structure parameters and the characteristic quantities of proposed PCFs at the pump wavelength.

| #               | $D_c$<br>( $\mu\text{m}$ ) | $\Lambda$<br>( $\mu\text{m}$ ) | $d_1/\Lambda$ | Pump wavelength<br>( $\mu\text{m}$ ) | $\text{Re}[n_{\text{eff}}]$ | $D$<br>( $\text{ps}/\text{nm.km}$ ) |
|-----------------|----------------------------|--------------------------------|---------------|--------------------------------------|-----------------------------|-------------------------------------|
| #F <sub>1</sub> | 1.314                      | 0.9                            | 0.45          | 1.55                                 | 1.384                       | 2.935                               |
| #F <sub>2</sub> | 1.4                        | 1.0                            | 0.5           | 1.55                                 | 1.39                        | 0.462                               |
| #F <sub>3</sub> | 1.34                       | 1.0                            | 0.55          | 1.3                                  | 1.406                       | -0.341                              |

The structure parameters and the characteristic quantities of the proposed PCFs at the pump wavelength are indicated in Tab.3. Dispersion values at the pump wavelength are much smaller than some previous work [20, 22, 28–29] on SC generation based on liquid-filled hollow-core PCFs.

## 4 Conclusion

We have investigated the circular lattice PCF structure with toluene infiltration. A near-zero ultra-flattened dispersion as small as 0.462 ps/(nm.km) is obtained over a broadband of 500 nm with the modification of structure parameters, in which the distance from the core to the air-holes of the first ring is suitably adjusted. The fibers also have a smaller and flatter dispersion than those with liquid infiltration in previous works [17, 20, 22, 28–29]. Moreover, the diversity in dispersion helps us to have many optimal fiber options to study SC generation as well as fabricate experimental fibers. Three optimal fibers with flat and small dispersion have been selected and analyzed in detail to be used for SC generation with broad bandwidths and low peak power.

## Acknowledgement

This research is funded by Vietnam's Ministry of Education and Training under grant number B2021-DHH-08.

## References

1. Alfano RR, Shapiro SL. Emission in the region 4000–7000 Å via four-photon coupling in glass. *Phys Rev Lett.* 1970;24(11):584-587.
2. Dupont S, Petersen C, Thøgersen J, Agger C, Bang O, Keiding SR. IR microscopy utilizing intense supercontinuum light source. *Opt. Express.* 2012;20(5):4887-4892.
3. Holzwarth R, Udem T, Hänsch TW, Knight JC, Wadsworth WJ, Russell PSJ. Optical frequency synthesizer for precision spectroscopy. *Phys Rev Lett.* 2000;85(1):2264-22267.
4. Shen Y, Voronin AA, Zheltikov AM, O'Connor SP, Yakovlev VV, Sokolov AV, et al. Supercontinuum generation in large-mode-area photonic crystal fibers for coherent Raman microspectroscopy. *Proc SPIE.* 2018;10522:105220I.
5. Travers JC, Chang W, Nold J, Joly NY, Russell PSJ. Ultrafast nonlinear optics in gas-filled hollow-core photonic crystal fibers. *J Opt Soc Am B.* 2011;28(12):A11-A26.
6. You YJ, Wang C, Lin YL, Zaytsev A, Xue P, Pan CL. Ultrahigh-resolution optical coherence tomography at 1.3 μm central wavelength by using a supercontinuum source pumped by noise-like pulses. *Laser Phys Lett.* 2016;13(2):025101.
7. Schliesser GA, Picqué N, Hänsch TW. Mid-infrared frequency combs. *Nat Photon.* 2012;6(7):40-449.
8. Lu R, Beers RV, Saeys W, Li C, Cen H. Measurement of optical properties of fruits and vegetables: a review. *Postharvest Biol. Technol.* 2020;159:111003.
9. Halloran M, Traina N, Choi J, Lee T, Yoo J. Simultaneous measurements of light hydrocarbons using supercontinuum laser absorption spectroscopy. *Energy Fuels.* 2020;34:3671-3678.
10. Sanchez-Cano A, Saldana-Diaz JE, Perdices L, Pinilla I, Salgado-Remacha FJ, Jarabo S. Measurement method of optical properties of ex vivo biological tissues of rats in the near-infrared range. *Appl Opt.* 2020;59:D111-D117.
11. Paul BK, Ahmed K, Asaduzzaman S, Islam MS. Folded cladding porous shaped photonic crystal fiber with high sensitivity in optical sensing applications: design and analysis. *Sens. Bio-Sens. Res.* 2017;12:36-42.
12. Nair AA, Jayaraju M. Design and study on square lattice-based photonic crystal fibre under different air holes for supercontinuum generation. *Pramana - J Phys.* 2018;91:66.
13. Hossain MdS, Sen S, Hossain MdM. Performance analysis of octagonal photonic crystal fiber (O-PCF) for various communication applications. *Physica Scripta.* 2021;96(5):55506.
14. Cai W, Liu E, Feng B, Xiao W, Liu H, Wang Z, et al. Dodecagonal photonic quasi-crystal fiber with high birefringence. *Journal of the Optical Society of America A.* 2016;33(10):2108-2114.

15. Vigneswaran D, Rajan MSM, Biswas B, Grover A, Ahmed K, Pau BK. Numerical investigation of spiral photonic crystal fiber (S-PCF) with supporting high order OAM modes propagation for space division multiplexing applications. *Opt Quant. Electron.* 2021;53:78.
16. Chemnitz M, Gaida C, Gebhardt M, Stutzki F, Kobelke J, Tünnermann A, et al. Carbon chloride-core fibers for soliton mediated supercontinuum generation. *Opt Express.* 2018;26(3):3221.
17. Lanh CV, Thuy HV, Van CL, Borzycki K, Khoa DX, Vu TQ, et al. Optimization of optical properties of photonic crystal fibers infiltrated with chloroform for supercontinuum generation. *Laser Phys.* 2019;29(7):075107.
18. Yan Chen G, Jinhui Y, Kuiru W, Haiyun W, Yujun C, Xian Z, et al. Generation of supercontinuum and frequency comb in a nitrobenzene-core photonic crystal fiber with all-normal dispersion profile. *Opt Commun.* 2021;481: 126555.
19. Junaid S, Bierlich J, Hartung A, Meyer T, Chemnitz M, Schmidt MA. Supercontinuum generation in a carbon disulfide core microstructured optical fiber. *Opt Express.* 2021;29:19891-19902.
20. Quang HD, Pniewski J, Hieu LV, Ramaniuk A, Van CL, Borzycki K, et al. Optimization of optical properties of photonic crystal fibers infiltrated with carbon tetrachloride for supercontinuum generation with subnanosecond femtosecond pulses. *Appl Opt.* 2018;57(14):3738-3746.
21. Bao Tran LT, Thuy NT, Ngoc VTM, Trung LC, Minh LV, Van CL, Khoa DX, Lanh CV. Analysis of dispersion characteristics of solid-core PCFs with different types of lattice in the claddings, infiltrated with ethanol. *Photon. Lett. Poland.* 2020;12(4):106-108.
22. Medjouri A, Simohamed LM, Ziane O, Boudrioua A, Becer Z. Design of a circular photonic crystal fiber with flattened chromatic dispersion using a defected core and selectively reduced air holes: Application to supercontinuum generation at 1.55  $\mu\text{m}$ . *Photonics and Nanostructures - Fundamentals and Applications.* 2015;16:43-50.
23. Maji PS, Chaudhuri PR. Supercontinuum generation in ultra-flat near zero dispersion PCF with selective liquid infiltration. *Optik.* 2014;125(20):5986-5992.
24. Huang T, Wei Q, Wu Z, Wu X, Huang P, Cheng Z, et al. Ultra-flattened normal dispersion fiber for supercontinuum and dissipative soliton resonance generation at 2  $\mu\text{m}$ , *IEEE Photon J.* 2019;11(3):7101511.
25. Huang T, Huang P, Cheng Z, Liao J, Wu X, Pan J. Design and analysis of a hexagonal tellurite photonic crystal fiber with broadband ultra-flattened dispersion in mid-IR. *Optik.* 2018;167:144-149.
26. Ho PP, Alfano RR. Optical Kerr effect in liquids. *Phys Rev A.* 1979;20(5):2170-2187.
27. Kato T, Suetsugu Y, Takagi M, Sasaoka E, Nishimura M. Measurement of the nonlinear refractive index in optical fiber by the cross-phase-modulation method with depolarized pump light. *Opt Lett.* 1995;20(9):988-990.
28. Lanh CV, Anuszkiewicz A, Ramaniuk A, Kasztelan R, Khoa DX, Van CL, et al. Supercontinuum generation in photonic crystal fibres with core filled with toluene. *J Opt.* 2017;19(12):125604.
29. Thuy NT, Duc HT, Bao Tran LT, Trong DV, Lanh CV. Optimization of optical properties of toluene-core photonic crystal fibers with circle lattice for supercontinuum generation. *J Opt.* 2022.
30. Saitoh K, Florous NJ, Koshihara M. Theoretical realization of holey fiber with flat chromatic dispersion and large mode area: an intriguing defected approach. *Opt Lett.* 2006;31(1):26-28.
31. Moutzouris K, Papamichael M, Betsis SC, Stavrakas I, Hloupis G, Triantis D. Refractive, dispersive and thermo-optic properties of twelve organic solvents in the visible and near-infrared. *Appl Phys B: Lasers and Optics.* 2013;116(3):617-622.
32. Tan CZ. Determination of refractive index of silica glass for infrared wavelengths by IR spectroscopy. *J Non-Crystalline Solids.* 1998;223(1-2):158-163.
33. Lee YS, Lee CG, Bahloul F, Kim S, Oh K. Simultaneously achieving a large negative dispersion and a high birefringence over Er and Tm dual gain bands in a square lattice photonic crystal fiber. *J Lightwave Technol.* 2019;37(4):1254-1263.
34. Moutzouris K, Papamichael M, Betsis SC, Stavrakas I, Hloupis G, Triantis D. Refractive, dispersive and thermo-optic properties of twelve organic solvents in the visible and near-infrared. *Appl Phys B.* 2013;116(3):617-622.